



## Imaging of a Circumsolar Dust Ring Near the Orbit of Venus

M. H. Jones *et al.*

*Science* **342**, 960 (2013);

DOI: 10.1126/science.1243194

*This copy is for your personal, non-commercial use only.*

If you wish to distribute this article to others, you can order high-quality copies for your colleagues, clients, or customers by [clicking here](#).

Permission to republish or repurpose articles or portions of articles can be obtained by following the guidelines [here](#).

**The following resources related to this article are available online at [www.sciencemag.org](http://www.sciencemag.org) (this information is current as of February 25, 2014 ):**

**Updated information and services**, including high-resolution figures, can be found in the online version of this article at:

<http://www.sciencemag.org/content/342/6161/960.full.html>

**Supporting Online Material** can be found at:

<http://www.sciencemag.org/content/suppl/2013/11/20/342.6161.960.DC1.html>

This article **cites 22 articles**, 2 of which can be accessed free:

<http://www.sciencemag.org/content/342/6161/960.full.html#ref-list-1>

This article appears in the following **subject collections**:

Planetary Science

[http://www.sciencemag.org/cgi/collection/planet\\_sci](http://www.sciencemag.org/cgi/collection/planet_sci)

14. A. Zweig, R. G. Fischer, J. E. Lancaster, *J. Org. Chem.* **45**, 3597–3603 (1980).
15. H. Schroeder *et al.*, *J. Org. Chem.* **27**, 2580–2584 (1962).
16. Commercial AgF<sub>2</sub> is a black crystalline solid.
17. The direct fluorination of pyridines with F<sub>2</sub> gas has been reported to occur in 31 to 70% yields with alkyl, chloro, and ester substituted pyridines. The direct fluorination of pyridines containing benzyl acyl, or bromo substituents with F<sub>2</sub> gas resulted in less than 30% yield. See (5–7).
18. The presence of five-membered aromatic heterocycles is not tolerated in the fluorination of pyridines.
19. D. K. Leahy *et al.*, *Org. Process Res. Dev.* **16**, 244–249 (2012).
20. T. Güngör, F. Marsais, G. Queguiner, *J. Organomet. Chem.* **215**, 139–150 (1981).
21. L. Estel, F. Marsais, G. Queguiner, *J. Org. Chem.* **53**, 2740–2744 (1988).
22. C. Bobbio, M. Schlosser, *J. Org. Chem.* **70**, 3039–3045 (2005).
23. H. I. Bradlow, C. A. Vanderwerf, *J. Org. Chem.* **14**, 509–515 (1949).
24. Y. H. Cherng, *Tetrahedron* **58**, 4931–4935 (2002).
25. A. Kling *et al.*, *Bioorg. Med. Chem.* **11**, 1319–1341 (2003).
26. S. Thomas, S. Roberts, L. Pasumansky, S. Gamsey, B. Singaram, *Org. Lett.* **5**, 3867–3870 (2003).
27. T. Kauffmann, A. Mitschker, A. Woltermann, *Chem. Ber.* **116**, 992–1000 (1983).
28. A. Loupy, N. Philippon, P. Pigeon, H. Galons, *Heterocycles* **32**, 1947 (1991).
29. In CD<sub>3</sub>CN; <sup>1</sup>H resonances for Me<sub>3</sub>py: δ 6.83, 2.38, and 2.23 ppm. <sup>1</sup>H resonances for Me<sub>3</sub>py + AgF<sub>2</sub>: δ 7.10, 2.59, and 2.32 ppm.
30. H. Meinert, *Z. Chem.* **5**, 64 (1965).
31. T. Umemoto, G. Tomizawa, *Tetrahedron Lett.* **28**, 2705–2708 (1987).
32. T. Umemoto, G. Tomizawa, *J. Org. Chem.* **54**, 1726–1731 (1989).
33. T. Umemoto, G. Tomizawa, H. Hachisuka, M. Kitano, *J. Fluor. Chem.* **77**, 161–168 (1996).
34. A. S. Kiselyov, L. Strekowski, *Synth. Commun.* **24**, 2387–2392 (1994).
35. F. Minisci, E. Vismara, F. Fontana, *Heterocycles* **28**, 489 (1989).
36. F. O'Hara, D. G. Blackmond, P. S. Baran, *J. Am. Chem. Soc.* **135**, 12122–12134 (2013).
37. Y. Fujiwara *et al.*, *Nature* **492**, 95–99 (2012).
38. D. A. Nagib, D. W. C. MacMillan, *Nature* **480**, 224–228 (2011).
39. It is likely that AgF combines with the liberated HF to form silver bifluoride (AgHF<sub>2</sub>).
40. E. Piers, M. Soucy, *Can. J. Chem.* **52**, 3563–3564 (1974).
41. P. B. Kraikivskii *et al.*, *J. Organomet. Chem.* **694**, 3912–3917 (2009).
42. P. B. Kraikivskii, H. F. Klein, V. V. Saraev, N. E. Schlörer, V. V. Bocharova, *J. Organomet. Chem.* **696**, 3376–3383 (2011).
43. P. B. Kraikivskii *et al.*, *J. Organomet. Chem.* **715**, 43–47 (2012).
44. D. Andrae, U. Häussermann, M. Dolg, H. Stoll, H. Preuss, *Theor. Chim. Acta* **77**, 123 (1990).
45. T. W. Bell, L. Y. Hu, S. V. Patel, *J. Org. Chem.* **52**, 3847–3850 (1987).
46. T. Honda, H. Namiki, M. Kudoh, H. Nagase, H. Mizutani, *Heterocycles* **59**, 169 (2003).

**Acknowledgments:** We thank the NIH (R37GM-55382) for support of this work and Chevron for a fellowship to P.S.F. A provisional patent application has been filed on this reaction.

#### Supporting Online Material

www.sciencemag.org/content/342/6161/956/suppl/DC1

Materials and Methods

Table S1

References (47–56)

25 July 2013; accepted 22 October 2013

10.1126/science.1243759

# Imaging of a Circumsolar Dust Ring Near the Orbit of Venus

M. H. Jones,<sup>1\*</sup> D. Bewsher,<sup>2</sup> D. S. Brown<sup>2</sup>

The gravitational interaction of dust in the zodiacal cloud with individual planets is expected to give rise to ringlike features: Such a circumsolar ring has been observed associated with Earth, but such resonance rings have not been confirmed to exist for other planets. Here, we report on sensitive photometric observations, based on imaging from the STEREO mission, that confirm the existence of a dust ring at the orbit of Venus. The maximum overdensity of dust in this ring, compared to the zodiacal cloud, is ~10%. The radial density profile of this ring differs from the model used to describe Earth's ring in that it has two distinct steplike components, with one step being interior and the other exterior to the orbit of Venus.

A circumsolar dust ring is known to exist around the orbit of Earth (1, 2). It arises from the trapping of interplanetary dust grains, primarily of asteroidal and cometary origin (3–5), into orbits that are resonant with Earth's orbit. Dust grains of sizes from 1 to 100 μm are subject to Poynting-Robertson (P-R) drag and to a lesser extent solar wind drag, which results in a gradual decay of their orbits [about 10<sup>4</sup> years for a 10-μm particle at 1 astronomical unit (AU)] (6). As a dust grain slowly spirals inward toward the orbit of the Earth, it successively passes into locations in which it may be trapped temporarily (for time scales of 10<sup>4</sup> to 10<sup>5</sup> years) into a particular orbital resonance (1, 7–9). Dust in individual resonances will cluster into periodic patterns around the orbit, and, when multiple resonances combine to form a real dust ring, these underlying structures result in the azimuthal distribution of the ring being nonuniform (1).

Searches for resonance structures around the orbits of Mars and Jupiter have not yet been successful (10). The situation at Venus is more complex. A detection of enhanced scattering was reported (11) from Venera 9 and 10 but is attributed to circumplanetary rather than circumsolar dust. On the basis of a reanalysis of photometry from the Helios mission, data consistent with a dust ring just outside the orbit of Venus have been presented (12), but the existence of such a ring could not be confirmed beyond doubt.

A circumsolar dust ring at Venus would provide observational data, which should lead to improved understanding of the factors affecting the formation of resonance rings, such as (P-R and solar wind) drag forces, an elliptical planetary orbit, and gravitational perturbation by an exterior planet (1, 7, 8). Furthermore, understanding of circumstellar dust rings is important in the context of exoplanetary systems (13). Not only are they an important consideration in proposed space-based interferometric imaging of exoplanets (14), large scale rings have been imaged directly, as in the case of Fomalhaut (15). Here, we describe a search for a ring at the

orbit of Venus based on photometry from an exterior viewpoint.

The STEREO mission (16), launched in October 2006, uses two nearly identical spacecraft, A and B, to provide synoptic observations of the Sun and the heliosphere interior to 1 AU. Each spacecraft carries a Heliospheric Imager instrument (17), HI-2, both of which continuously monitor the inner zodiacal cloud. These HI-2A and HI-2B instruments have a field of view of about 70° centered on ecliptic latitude β ≈ 0° at heliocentric longitude |λ'| = 53.7°. In searching for a dust ring at the orbit of Venus, the lines of sight that are of interest are close to the ecliptic plane and have 40° < |λ'| < 50° (depending on the location of the spacecraft) (Fig. 1).

In normal science operations, the HI-2 instrument generates a 1024 pixel-by-1024 pixel image with ≈4-arc min resolution every 2 hours. Further processing, including positional calibration (18), results in the level-1 data used here. The instrument is sensitive to wavelengths of 400 to 1000 nm, and the dominant diffuse source in HI-2 images is solar radiation scattered by dust grains [with radii of 10 to 100 μm (19)] in the zodiacal cloud. The typical surface brightness at (λ' ≈ 45°, β ≈ 0°) is ≈8 DN s<sup>-1</sup> pixel<sup>-1</sup> [DN is data number, 1 DN ≈ 15 photoelectrons is the default unit used by the instrument team (17)]. The HI-2 instrument was designed (17) to monitor coronal mass ejections having a surface brightness of about 1% of that of the zodiacal light. By combining ~100 HI-2 level-1 images, photometry on the zodiacal cloud to an accuracy of order 0.1% can be extracted. A major limitation is the presence of systematic errors that compromise this photometry. These arise from various sources: saturation stripes, ghosting caused by bright objects, and the presence of the galactic plane within 30° of the region of interest. To avoid contamination, data containing these features were not used in our analysis.

Photometry of HI-2 data involved combining level-1 images from 10 consecutive days (i.e., up to

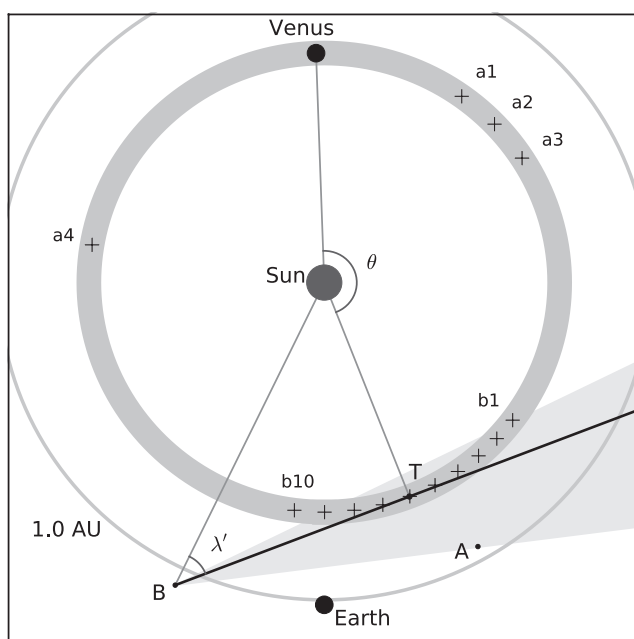
<sup>1</sup>Department of Physical Sciences, The Open University, Walton Hall, Milton Keynes, Buckinghamshire MK7 6AA, UK. <sup>2</sup>Jeremiah Horrocks Institute, University of Central Lancashire, Preston, Lancashire PR1 2HE, UK.

\*Corresponding author. E-mail: m.h.jones@open.ac.uk

120 images, with an integrated exposure time of  $\approx 8$  days). Surface brightnesses were determined over a grid with extent  $|\beta| < 8.5^\circ$  and  $35.0^\circ < \lambda' <$

$60.0^\circ$  (HI-2A) or  $-60.0^\circ < \lambda' < -35.0^\circ$  (HI-2B), with cell size of  $0.5^\circ$  in  $\lambda'$  and  $1.0^\circ$  in  $\beta$ . For each cell, the cumulative probability distribution of

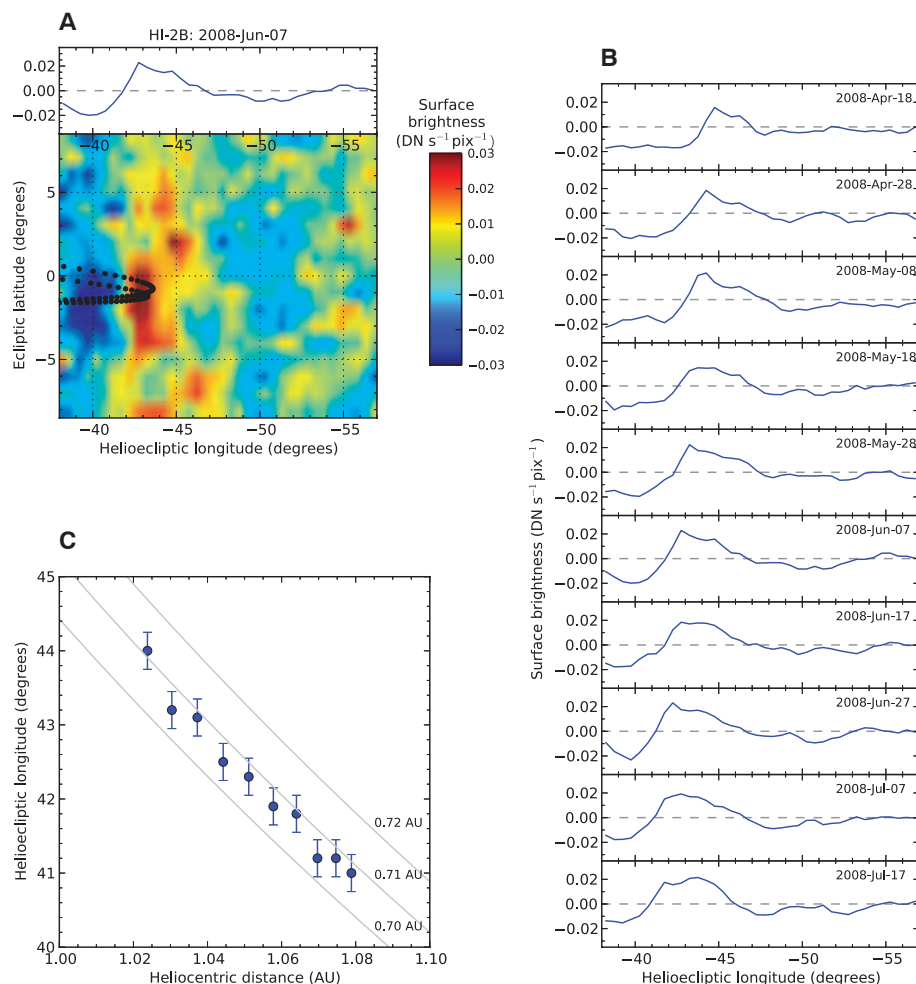
**Fig. 1. The viewing geometry (from ecliptic north) of a circumsolar dust ring at Venus from STEREO-B.** Planet and STEREO spacecraft (A and B) positions are for 12 June 2008. A ring at the orbit of Venus (thick gray band) is viewed tangentially from B along a line of sight passing through T. The range of helioecliptic longitude  $\lambda'$  mapped is indicated (pale gray). Crosses indicate the locations of T in the observations presented here. The start dates of the STEREO-A data sets are (a1) 9 June 2009, (a2) 29 June 2009, (a3) 19 July 2009, and (a4) 12 November 2008. There are 10 consecutive sets of STEREO-B data: (b1) 18 April to (b10) 17 July 2008.



surface brightness was determined by using the image pixels within that cell (typically  $\approx 14,000$  values). The surface brightness of each cell was estimated as that corresponding to a probability of 0.45 (a value slightly lower than the median is expected due to the presence of point sources). This grid was treated as a series of independent scans at constant  $\beta$ , which were fitted to a power law,  $k|\lambda'|^{-n}$  (20). Each scan was detrended by using a box-car filter of width  $6.5^\circ$  (i.e., 13 cells of  $0.5^\circ$  width), followed by subtraction of the result of applying the filter to the best-fitting power law for that scan. The resultant scans are used in two ways: as a map of extent  $38.0^\circ \leq |\lambda'| \leq 57.0^\circ$  and  $|\beta| \leq 8.5^\circ$  and as a mean scan along the ecliptic plane (covering  $38.0^\circ \leq |\lambda'| \leq 57.0^\circ$ ) by averaging over  $|\beta| \leq 4.5^\circ$ .

An example map from a 10-day observation period of HI-2B data starting on 7 June 2008 00:00 UTC (all data sets are referred to by their starting date) shows a bright feature coincident with the tangent to the orbit of Venus (Fig. 2A). This is as expected for a dust ring along a line of sight where the dust column density is maximized (Fig. 1; the position of the tangent point with respect to Venus is given by the azimuthal angle  $\theta$ ). Given the sensitivity of these maps to systematic errors, this is in itself insufficient to

**Fig. 2. A bright feature and its change of position with varying heliocentric distance of the STEREO-B spacecraft.** (A) The surface brightness map (bottom) and mean scan (top) of a 10-day integration of HI-2B data starting on 7 June 2009 00:00 UTC. The orbit of Venus as viewed from STEREO-B at the start and the end of the integration time is shown by black dots. Surface brightness is expressed in  $\text{DN s}^{-1} \text{pixel}^{-1}$  [pixels are those of the charge-coupled device (CCD) of the HI-2 instrument]. (B) Surface brightness mean scans for a sequence of 10 10-day periods (b1 to b10 in Fig. 1) starting on 18 April 2008 00:00 UTC. (C) The helioecliptic longitude of the midrise point on the sunward side of the peaks in (B) against the heliocentric distance of STEREO-B. The gray curves show the expected behavior if the feature is associated with a physical ring at the indicated radii. Error bars indicate  $1\text{-}\sigma$  measurement uncertainties.



demonstrate beyond doubt the existence of such a ring. However, when the same detrending method is applied to a region ( $-67.0^\circ \leq \lambda' \leq -48.0^\circ$ ) that does not contain the orbit of Venus, no such bright feature is detected (fig. S1).

Furthermore, this data set is just one from a 100-day interval (starting 18 April 2008) from

which 10 consecutive data sets (b1 to b10 in Fig. 1) could be analyzed. In the mean scans of this sequence (Fig. 2B), the helioelectric longitude of the feature decreases with time. Because of the spacecraft orbit, the heliocentric distance,  $r$ , of STEREO-B varied from 1.02 to 1.08 AU over this interval. The view of a physical feature would be

expected to change with viewing position, with  $|\lambda'|$  decreasing as  $r$  increases. The position of the feature was determined (to an accuracy of  $\approx 0.25^\circ$ ) by reference to the point at which the surface brightness is midway between the peak and minimum value on the sunward side. Figure 2C shows these positions against  $r$ . The behavior is

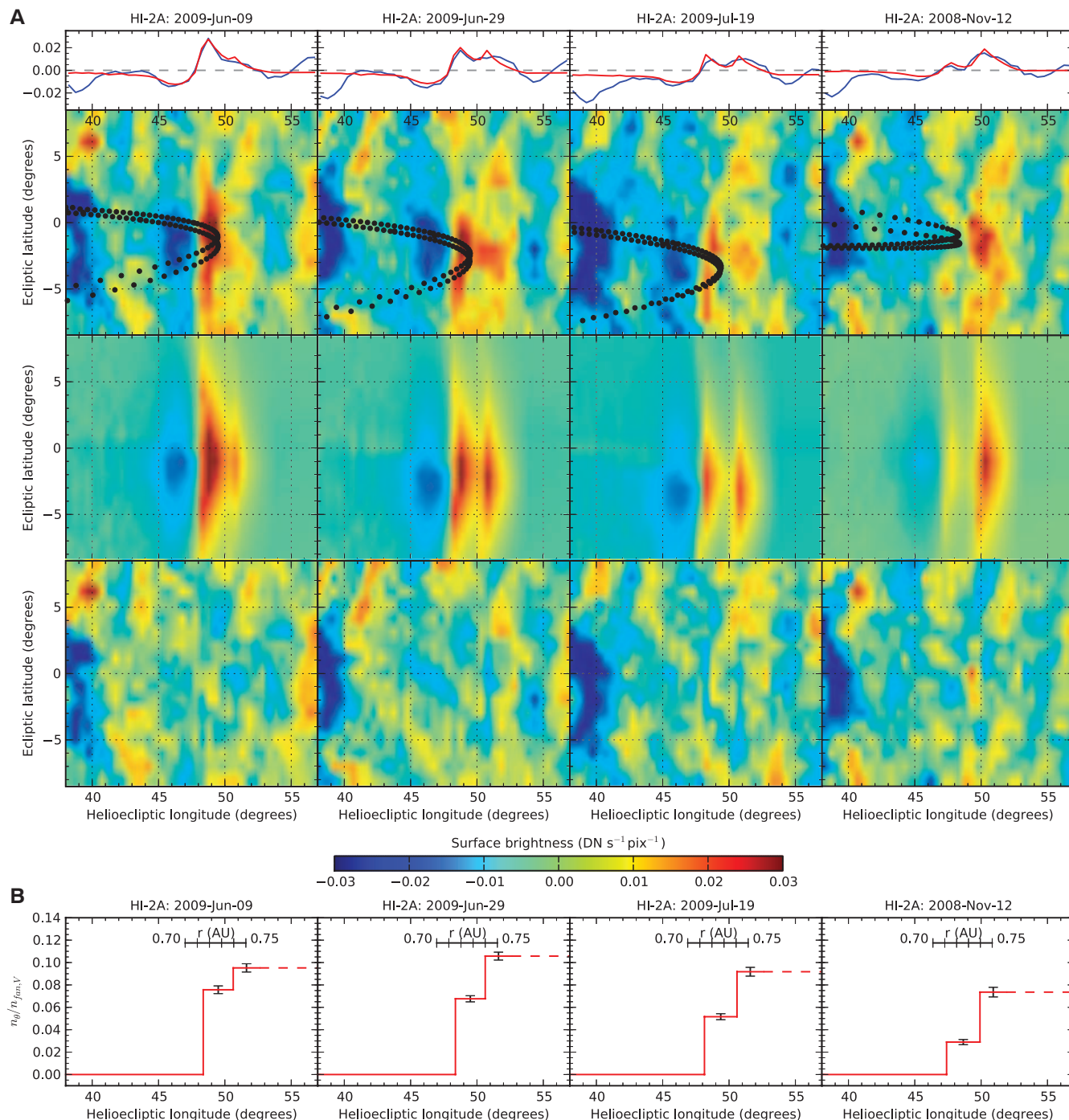


**Fig. 3. Surface brightness mean scans and maps and model radial density profiles for HI-2A data sets starting at 00:00 UTC on 9 June, 29 June, and 19 July 2009 and 12 November 2008. (A)** From the top downward: top, mean scans (blue) with best-fitting models (red); second row, maps from the data; third row, maps of the best-fitting models;

bottom row, residual (data minus model) maps. Units are as in Fig. 2A. **(B)** The fitted radial density profiles for the two-step density model shown in (A). The profile is plotted against the helioelectric longitude of the tangent point of a ring with heliocentric radius ( $r$ ). Density is expressed in terms of  $n_{\text{H}}/n_{\text{fan},V}$ . Error bars show the 1- $\sigma$  uncertainties of the fitted densities.



as expected for a physical ring located close to the orbit of Venus. Last, there are observations from STEREO-A that view the same tangent point ( $\theta = 170^\circ$ ) as the 17 July 2008 data. Again, an extended feature is observed close to the orbit of Venus (fig. S2), further supporting the view that it arises from a physical structure at this location.

In the sequence of mean scans (Fig. 2B),  $\theta$  changes by  $\approx 60^\circ$ ; hence, the feature appears to be an arc occupying a substantial fraction of the orbit. In conjunction with further HI-2A data that also show a bright feature near the orbit of Venus (Fig. 3A) but that are  $\approx 120^\circ$  away in  $\theta$  from the HI-2B data (Fig. 1), these data are indicative of a ring (or a series of arcs) that is associated with the orbit of Venus.

The mean scans in Fig. 2B allow some inferences to be made about the underlying dust density distribution. The bright feature is asymmetric, with a steeper decline on the sunward side than its other side. This rules out models in which the variation of dust density with  $r$  is symmetric around some fixed radius [as in the Gaussian model (21) of Earth's ring], which would exhibit a peak with the shallower decline on its sunward side.

The majority of the mean scans (Fig. 2B) show evidence of a double-peak structure (e.g., 8 May 2008), but there are mean scans from HI-2A data (Fig. 3A) that more clearly reveal the existence of two components to the peak profile. The data from 9 June 2009 display a strong sharp peak slightly interior to the orbit of Venus but with a shallow decline exterior to the orbit. By 29 June 2009, the sharp peak has reduced in intensity, whereas the gradual decline has changed into a second peak. By 19 July 2009, there are two very distinct peaks in the mean scan profile. An earlier observation, 12 November 2008, shows that the interior peak can be weak, whereas the exterior peak is relatively strong. Therefore, there appear to be two distinct components to the ring, one just inside and one exterior to the orbit of Venus. Furthermore, the absolute and relative intensities of these two components show considerable variation with  $\theta$ .

To characterize this observed behavior, we adopted a simple parametric model to describe the dust density distribution (22). The model is defined in terms of coordinates ( $r, z, \theta$ ), in which  $z$  is the vertical distance from the plane of the ring. The vertical behavior is modeled as an exponential distribution with scale height  $\sigma_z$  (21). The radial dependence is one in which the density changes in two sharp steps (at  $r_0$  and  $r_1$ ), so the dust density in the ring is  $n_\theta(r)e^{-|z|/\sigma_z}$ , where

$$n_\theta(r) = \begin{cases} 0, & r < r_0 \\ n_{0,\theta}, & r_0 < r < r_1 \\ n_{1,\theta}, & r_1 < r \end{cases} \quad (1)$$

A limitation of this model is that the ring density should drop to zero as  $r$  increases beyond  $r_1$ . Such a decline cannot be discerned in the maps because of the spatial filtering used. Accepting this limitation, this two-step model was

adopted because it provides an indication of the sharp density changes that appear to be present.

The ring is assumed to be coplanar with the orbit of Venus, and a phase function for optical scattering (23) is adopted. In fitting this model to the maps, the variable parameters were  $n_{0,\theta}$ ,  $n_{1,\theta}$ ,  $r_0$ , and  $r_1$  (table S1). The scale height was fixed at the weighted mean (of the HI-2A observations) value of  $\sigma_z = 0.055$  AU, noting that genuine variation in  $\sigma_z$  with  $\theta$  cannot be ruled out.

The two-step model provides an adequate description of the data as shown (Fig. 3A) in the data, model, and residual (compare with the no-signal map of fig. S1) maps. There are some discrepancies, most notably that the outer step in the model has a sharper peak than is observed, but overall the model reproduces the range of observed behavior by variation of a small number of parameters.

Overall, the ring densities are up to  $\sim 10\%$  of the density  $n_{\text{fan},V}$  of the smooth cloud (at its symmetry plane) (24). The difference in profiles between 9 June 2009 and 19 July 2009 can be explained in the two-step model by the variation of the relative difference between the first and second density steps. The profile with a very sharp interior peak (9 June 2009) has  $n_{0,\theta} \approx 0.8 n_{1,\theta}$ . As the sequence of observations progresses,  $n_{0,\theta}/n_{1,\theta}$  decreases to  $\approx 0.57$ , resulting in a double-peak profile by 19 July 2009. The data from 12 November 2008, in which the inner component was weak, has  $n_{0,\theta} \approx 0.4 n_{1,\theta}$ . Furthermore, the absolute densities show variation between this observation and the 2009 June and July observations:  $n_{1,\theta} = 0.074 n_{\text{fan},V}$  for the former, whereas  $n_{1,\theta} \approx 0.10 n_{\text{fan},V}$  for the latter. This is in qualitative agreement with the prediction (1) that the greater drag experienced by dust at the orbit of Venus and the higher orbital speeds should result in a ring that is less pronounced than Earth's ring [which has an overdensity of about 0.16 (21)]. Also, the data of 2009 June and July represent small (negative) values of  $\theta$  ( $-38^\circ$  to  $-59^\circ$ ) (25), and the relatively high values of  $n_{0,\theta}$  and  $n_{1,\theta}$  may reflect a density enhancement similar to the so-called trailing blob observed in Earth's ring (21, 26).

The radii  $r_0$  and  $r_1$  are well constrained and do not exhibit much variation between different data sets.  $r_0$  is not only interior to the semimajor axis of the orbit of Venus (0.7233 AU), it is also interior to the perihelion distance of Venus (0.7184 AU). Likewise, the location of the second step,  $r_1$ , is exterior to the aphelion distance of Venus (0.7282 AU). Numerical simulations (14) of resonance rings in exozodiacal clouds predict a sharp change in ring surface density interior to the planetary orbit. In particular, where the ring density contrast exceeds 30% (which admittedly is not the case for the Venus ring), the inner edge is at  $\approx 0.83$  of the semimajor axis of the planetary orbit (14). Applied to Venus, this implies  $r_0 \approx 0.60$  AU—smaller than observed here. Additionally, a sharp increase in surface density at a radius exterior to the planetary orbit is apparent

in some ring simulations [see catalog (27) linked to (14)].

## References and Notes

1. S. F. Dermott, S. Jayaraman, Y. L. Xu, B. Å. S. Gustafson, J. C. Liou, *Nature* **369**, 719–723 (1994).
2. W. T. Reach *et al.*, *Nature* **374**, 521–523 (1995).
3. J. M. Hahn, H. A. Zook, B. Cooper, B. Sunkara, *Icarus* **158**, 360–378 (2002).
4. D. Nesvorný *et al.*, *Astrophys. J.* **713**, 816–836 (2010).
5. M. Rowan-Robinson, B. May, *Mon. Not. R. Astron. Soc.* **429**, 2894–2902 (2013).
6. J. A. Burns, P. L. Lamy, S. Soter, *Icarus* **40**, 1–48 (1979).
7. A. A. Jackson, H. A. Zook, *Nature* **337**, 629–631 (1989).
8. S. J. Weidenschilling, A. A. Jackson, *Icarus* **104**, 244–254 (1993).
9. A. J. Mustill, M. C. Wyatt, *Mon. Not. R. Astron. Soc.* **413**, 554–572 (2011).
10. M. J. Kushner, W. T. Reach, M. E. Brown, *Icarus* **145**, 44–52 (2000).
11. V. A. Krasnopolsky, A. A. Krysko, *Planet. Space Sci.* **27**, 951–957 (1979).
12. C. Leinert, B. Moser, *Astron. Astrophys.* **472**, 335–340 (2007).
13. M. J. Kushner, M. J. Holman, *Astrophys. J.* **588**, 1110–1120 (2003).
14. C. C. Stark, M. J. Kushner, *Astrophys. J.* **686**, 637–648 (2008).
15. P. Kalas, J. R. Graham, M. Clavin, *Nature* **435**, 1067–1070 (2005).
16. M. L. Kaiser *et al.*, *Space Sci. Rev.* **136**, 5–16 (2008).
17. C. Eyles *et al.*, *Sol. Phys.* **254**, 387–445 (2009).
18. D. S. Brown, D. Bewsher, C. J. Eyles, *Sol. Phys.* **254**, 185–225 (2009).
19. E. Grün, H. A. Zook, H. Fechtig, R. H. Giese, *Icarus* **62**, 244–272 (1985).
20. S. Kouchmy, P. L. Lamy, in *Properties and Interactions of Interplanetary Dust*, R. H. Giese, P. Lamy, Eds. (Reidel, Dordrecht, Netherlands, 1985), pp. 63–74.
21. T. Kelsall *et al.*, *Astrophys. J.* **508**, 44–73 (1998).
22. Materials and methods are available as supplementary materials on Science Online.
23. S. S. Hong, *Astron. Astrophys.* **146**, 67–75 (1985).
24.  $n_{\text{fan},V}$  was found using a modified fan model (21) with optical scattering (23) and scaled to match the mean surface brightness of the 9 June 2009 data.
25. The presence of Venus in the field of view precludes observations with  $|\theta| < 38^\circ$ .
26. W. T. Reach, *Icarus* **209**, 848–850 (2010).
27. <http://asd.gsfc.nasa.gov/Christopher.Stark/catalog.php>.

**Acknowledgments:** The HI instrument was developed by a collaboration that included the Rutherford Appleton Laboratory and the University of Birmingham, both in the United Kingdom; the Centre Spatial de Liège (CSL), Belgium; and the U.S. Naval Research Laboratory (NRL), Washington, DC. The STEREO/SECCHI (Sun Earth Connection Coronal and Heliospheric Investigation) project is an international consortium of the NRL (USA), Lockheed Martin Solar and Astrophysics Lab (USA), NASA Goddard Space Flight Center (USA), Rutherford Appleton Laboratory (UK), University of Birmingham (UK), Max-Planck-Institut für Sonnen-system-forschung (Germany), CSL (Belgium), Institut d'Optique Théorique et Appliquée (France), and Institut d'Astrophysique Spatiale (France). The HI-2 level-1 science data used in this study are available from [www.ukssdc.ac.uk/solar/stereo/data.html](http://www.ukssdc.ac.uk/solar/stereo/data.html).

## Supplementary Materials

[www.sciencemag.org/content/342/6161/960/suppl/DC1](http://www.sciencemag.org/content/342/6161/960/suppl/DC1)  
Materials and Methods  
Supplementary Text  
Figs. S1 and S2  
Table S1  
References

15 July 2013; accepted 28 October 2013  
10.1126/science.1243194